



Synthesis of ultrafast wavepackets with tailored spatiotemporal properties

Daniel Cruz-Delgado¹, Stephanos Yerolatsitis¹, Nicolas K. Fontaine [©]², Demetrios N. Christodoulides [©]¹, Rodrigo Amezcua-Correa^{1™} and Miguel A. Bandres [©]¹™

Sculpting light in space and time can provide unprecedented opportunities in many areas of science and technology, ranging from extreme nonlinear optics and quantum networks to new families of ultrafast fibre amplifiers. Although endeavours in accessing the light's temporal and spatial degrees of freedom have been carried out, controlling the electromagnetic field in its entirety has always been a major challenge. Here we demonstrate a versatile approach to synthesize convoluted ultrafast light structures in which the spatial and temporal dimensions are precisely correlated. By utilizing a two-stage reconfigurable module, we produce separable and non-separable trains of ultrafast wavepackets with time-varying dynamic angular momentum and tailored spectral characteristics. The generated light states are observed using mode- and frequency-resolved tomographic methodologies capable of reconstructing their complex field structure in space and time. Our results could have ramifications in a broad range of applications such as high-resolution microscopy, high-harmonic generation and laser micromachining.

Producing reconfigurable spatiotemporal wavepackets on request is nowadays one of the holy grails in photonics. Success in achieving this goal could have major implications in the rapidly developing fields of laser ignition systems and nanofabrication¹, quantum communications^{2,3}, mode-division multiplexing^{4,5} and machine learning⁶⁻⁸, among others. Spatiotemporal structured light can provide new capabilities in controlling light generation and propagation that, in turn, can be deployed to access new regimes in multimode amplification^{9,10}, extreme nonlinear optics¹¹, high-harmonic generation¹²⁻¹⁸ and laser micromachining^{19,20}. Historically, the prospect of shaping the temporal profile of a light packet emerged in the mid-80s within the context of pulse synthesis^{21,22}. Almost concurrently, the idea of suppressing diffraction effects by engineering the spatial complex wavefront was introduced, leading to the first experimental demonstration of Bessel beams²³. This, in turn, incited a flurry of activities in exploring other classes of non-diffractive beams24-26 and complex structures carrying orbital angular momentum (OAM) and topological charge²⁷. Earlier studies have also addressed the possibility of co-manipulating the space-time (ST) degrees of freedom (DOFs). Prominent examples of such ST waves include the extended family of X-waves²⁸ as well as other electromagnetic structures that simultaneously defy diffraction and dispersion effects like the Airy-Bessel optical bullets²⁹. In recent experimental demonstrations, ST wavepackets have been synthesized featuring specific correlations among the various DOFs. By adopting such emerging techniques, the frequencies and their corresponding \vec{k} vectors can be entangled, thus allowing the generation of a rich variety of single localized

spatiotemporal structures^{30–32} of ST vortices^{33–37} and toroidal vortices^{38,39}. Yet, despite this progress, controlling the field dynamics in its entirety, in a fully flexible manner, is an ongoing issue. Although, so far, isolated ST wavefronts had been routinely produced in various configurations and spatial modes have been multiplexed under continuous-wave conditions⁴⁰, the prospect of generating predefined and extended pulse trains with intertwined space/time variables still remains out of reach. Here we present a step forward in addressing this long-standing problem in optics. This is achieved by systematically accessing and tailoring the spatiotemporal dimensions of an ultrashort pulse-train beam through a sequence of spatial transformations on a spectrally modulated field (Fig. 1a). Our system tailors the spatial dimensions of the field by means of a highly customizable spatial-mode multiplexer with exceptionally high resolution. We intentionally engineer both temporal and spatial entities of the photon field ad libitum. The system presented in this work is totally reconfigurable in both frequency and space domains and is compatible with fibre technologies. To demonstrate the versatility of our approach, we synthesize non-separable (entangled) wave-train packets with time-varying OAM characteristics. Our results obtained at ~1 µm—a wavelength where most high-power fibre amplifiers operate at-can lead to a new generation of multimode ultrafast fibre sources. This concept can be readily adapted to support higher DOFs like polarization and OAM with very high vorticities. In this study, we also present a tomographic system capable of interrogating the generated light states.

Experimental setup

To tailor the spatiotemporal properties of an ultrafast field, we have developed the experimental platform shown in Fig. 1b. Light from a 180 fs laser source (~6.4 nm full-width at half-maximum (FWHM)) centred at ~1,030 nm is divided into two arms: a reference and a signal. During the first stage, the signal beam enters a two-dimensional Fourier-transform pulse shaper that enables us to simultaneously manipulate its spectral/temporal characteristics, whereas we can simultaneously reconfigure the field into an array of Gaussian beams on demand⁴¹. To achieve this, we use a folded pulse shaper architecture involving a diffraction grating, a cylindrical lens and a reflective spatial light modulator (SLM). In this arrangement, the long/horizontal dimension of the SLM is responsible for imprinting the desired spectral phase profiles, whereas the short/vertical dimension is utilized to controllably steer the ultrashort pulse to a specific output position by applying a linear phase. By encoding a superposition of multiple holograms into a single SLM phase mask, the two-dimensional Fourier-transform pulse shaper generates an array of spectrally modulated beams in the vertical direction. We NATURE PHOTONICS LETTERS

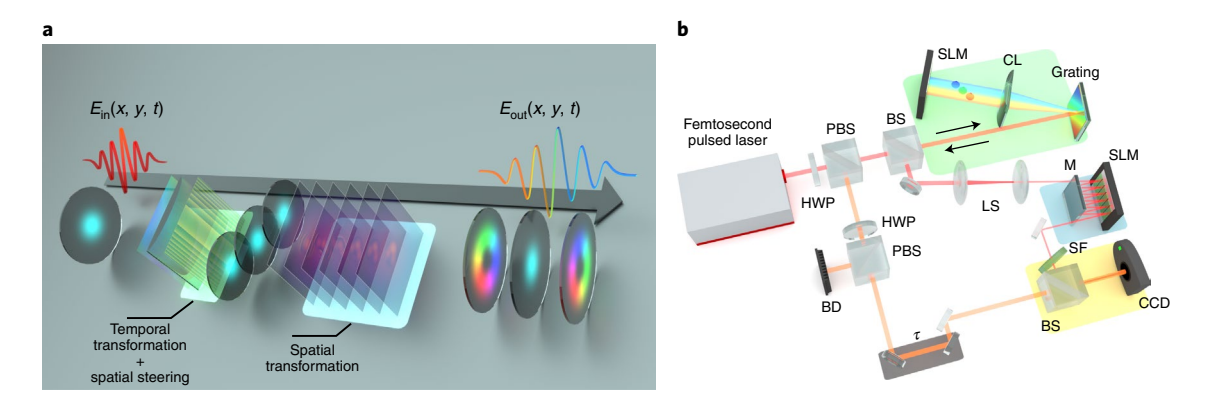


Fig. 1 | Spatiotemporal moulding of light. **a**, Conceptual scheme: an ultrafast pulse, $E_{in}(x, y, t)$, undergoes a series of spectral, temporal and spatial operations to synthesize spatiotemporal wavepackets featuring on-demand correlations among the various DOFs, $E_{out}(x, y, t)$. **b**, In the setup, the femtosecond pulse is divided into signal (red line) and reference (orange line) beams. A power control system composed of two sets of half-wave plates (HWPs) and polarization beamsplitters (PBSs) is used to control the energy on each arm. The unused energy is sent to a beam dump (BD). Initially, the signal pulse is manipulated in a spectral/temporal stage (green background). At this stage, a two-dimensional Fourier-transform pulse shaper composed of a diffraction grating, cylindrical lens (CL) and spatial light modulator (SLM) is employed to tailor the frequency components of the pulse by the horizontal axis of the SLM. Simultaneously, the vertical axis of the SLM is used to steer the spectrally modulated pulse to different spatial positions before entering a multiplane light conversion (MPLC) system. Encoding distinct holograms on the SLM allows us to create a set of vertical output spots. We then employ a two-lens system (LS) to condition the size of the beams before entering the stage where the field is spatially engineered. Subsequently, the field undergoes a spatial transformation in the next platform (blue background). The MPLC comprising an SLM and a mirror (M) is used to quasi-adiabatically mould the spatial phase and intensity profiles of the wavepacket. The synthesized spatiotemporal optical field, at the output, is analysed using a frequency-resolved tomographic interrogation module (yellow background). The holographic interference pattern between the reference arm, whereas the frequency components are interrogated by tilting a spectral filter (SF). Supplementary Sections II–V provide more details about this module.

then employ a two-lens system to condition the size of the beams before entering the stage where the field is spatially engineered. This stage is implemented via a unitary spatial transformation based on a multiplane light conversion (MPLC) system 42,43 , capable of converting the linear array of N Gaussian beams into a set of N co-propagating two-dimensional spatial modes. In the MPLC system, an SLM and a mirror allow the input field to bounce alternately between these two elements, impinging on a discrete set of six holograms employed to perform a quasi-adiabatic spatial shaping of the field. A key attribute of our ST wavepacket synthesis system is its ability to coherently combine the multiple Gaussian beams generated in the temporal shaping stage within the two-dimensional spatial mapping section. This powerful scheme allows one to have full access to the temporal and spatial DOF of the pulsed field.

In general, the optical field synthesized at one specific location $z=z_0$, in one polarization component, can be represented as a spatiotemporal superposition:

$$E_{0}(x, y, t) = \sum_{m,n,k} F_{(m,n),k}(t) \exp\left\{i\Psi_{(m,n),k}(t)\right\}$$

$$\exp\left\{i\omega_{k}t\right\} \operatorname{HG}_{(m,n),k}(x, y) \exp\left\{i\varphi_{(m,n),k}\right\},$$
(1)

where a set of carrier frequencies ω_k , labelled by k, are modulated by complex temporal envelope functions $F_{(m,n),k}(t) \exp\{i\Psi_{(m,n),k}(t)\}$, where each one is spatially structured through a corresponding Hermite–Gaussian mode $\mathrm{HG}_{(m,n),k}(x,y)$ and a spatial global phase $\varphi_{(m,n),k}$, where (m,n) are the spatial indices of the transverse modes. In this respect, we can generate an array of ST wavepackets with entangled ST DOFs that are not necessarily separable, that is, they cannot be simply expressed as E(x,y,t)=S(x,y)T(t). To interrogate the three-dimensional spatiotemporal composition of the synthesized ST optical fields, we use a spectrally resolved holographic technique that enables one to retrieve the complex (amplitude/phase) spatial composition of each spectral component at different time locations. For this purpose, the interference pattern between the signal and

reference waves is recorded with a charge-coupled device (CCD) camera within a Mach–Zehnder configuration at an off-axis geometry^{44,45}. We sequentially sweep the time delay of the reference beam to reconstruct the signal wave dynamics. Additionally, by using a controllably tilted narrow bandpass filter, we can discriminate the spectral components of the ST wave.

Wavepacket synthesis

To demonstrate the capabilities of our ST synthesis system, an ST wavepacket with a negative linear chirp ($\beta = 3.73 \times 10^{25} \,\mathrm{s}^{-2}$) is produced. In contrast to conventional ultrafast pulses, here we intentionally allocate different vorticities at different parts of the spectrum such that the short wavelengths of the spectrum are assigned to a spatial mode with vorticity $\ell = +1$ and the long wavelengths to an OAM mode with charge $\ell = -1$ (we generate the Laguerre basis as a linear combination of the Hermite-Gaussian modes as per the conventional decomposition performed elsewhere⁴⁶). This leads to a non-separable ultrashort pulse with a time-varying topological charge. To capture the convoluted composition of the fashioned ST wavefront, we interrogate the generated structure using spatial, temporal and frequency-resolved measurements. In Fig. 2a, we present the iso-intensity profile of the synthesized ST beam, reconstructed by considering all the spectral components at each specific time. The pulsed spatial intensity distribution has a vortex hollow cylindrical shape. Due to the intricate nature of this wavepacket, a conventional spectrogram cannot fully capture the field dynamics. To address this issue, we produced an enhanced pixelized spectro-temporal map (Fig. 2b). Each 'pixel' in this map displays the intensity and phase morphology of the ST wavepacket, when measured at a specific time and wavelength. The amplitude and phase are represented by brightness and colour, respectively (Supplementary Section I). To visualize these aspects in greater detail, Fig. 2c presents an expanded view of the intensity and phase distributions associated with two selected sections of the measured spectro-temporal map. The transition of the OAM content from $\ell = +1$ to $\ell = -1$ across different spectral/temporal regions is LETTERS NATURE PHOTONICS

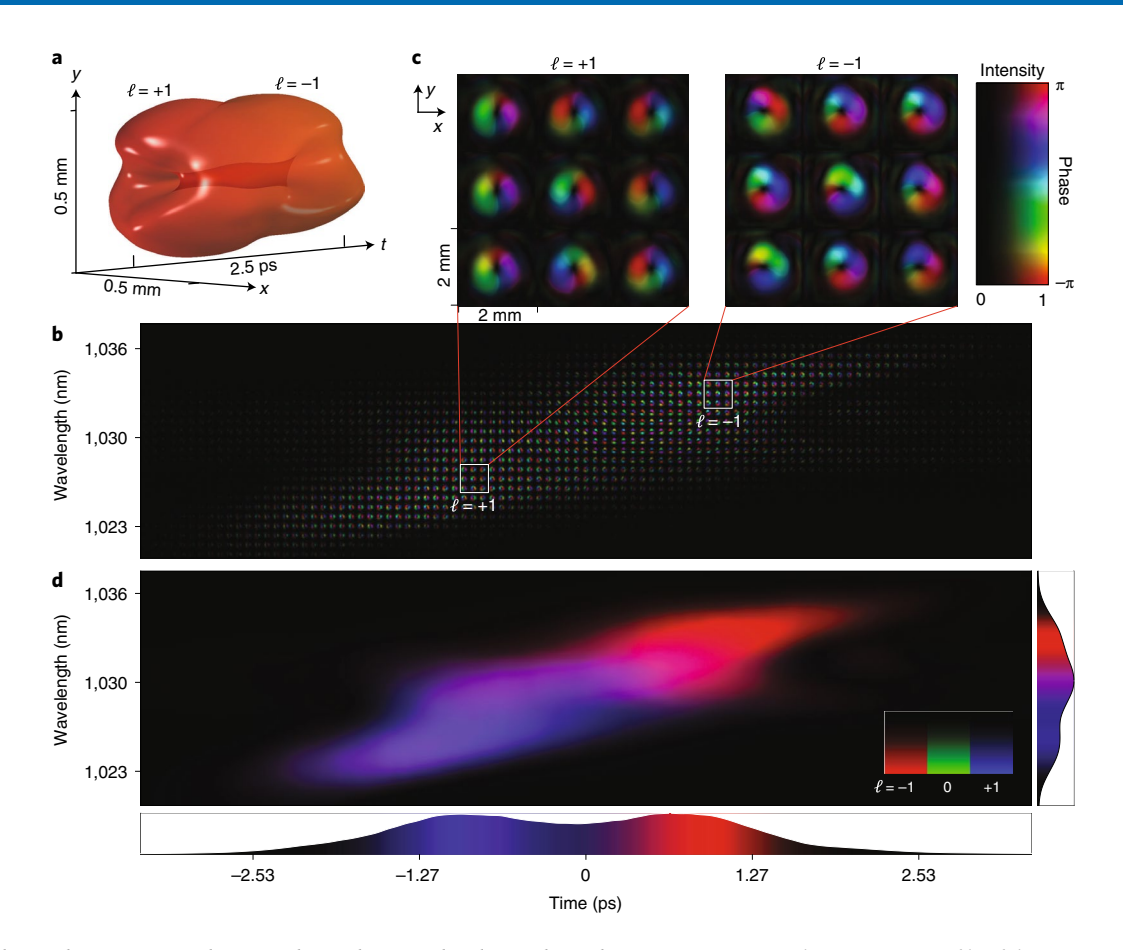


Fig. 2 | Synthesized spatiotemporal wavepacket with spectral and time-dependent OAM. a, Measured iso-intensity profile of the generated optical field (at $I_{\text{contour}} = 0.3I_{\text{max}}$) displaying a vortex structure $\ell = \pm 1$. b, Corresponding spectro-temporal map where each 'pixel' depicts the complex (amplitude/phase) spatial distribution measured at a specific time and wavelength. The amplitude and phase are represented by brightness and colour, respectively. c, Enlarged view of selected regions of the spectro-temporal map, showing vortex structures with opposite OAM. d, Colour-coded modal decomposition map after projecting the field onto a set of Laguerre–Gaussian modes. Each mode of this basis is associated with an RGB colour ($\ell = -1$ (red); $\ell = 0$ (green); $\ell = +1$ (blue)). The two distinct blue and red regions highlight the OAM variation along the pulse in both temporal and frequency axes. The total intensity profiles are also displayed on the same coordinates.

evident (Fig. 2b). To further analyse the properties of this pulse, we decompose each pixel in the map in the two-dimensional OAM Laguerre basis. By doing so, we can assign a red–green–blue (RGB) colour channel to each vorticity value (ℓ_{-1} =-1 (red); ℓ_0 =0 (green); ℓ_{+1} =+1 (blue)), creating an RGB additive colour model, in which any superposition of the three-colour channels is represented by a single colour (Supplementary Section VI). In Fig. 2d, we display the colour-coded modal decomposition as a wavelength/time map. We can clearly notice the two distinct colour regions, corresponding to the two different topological charges⁴⁶.

The ST synthesis system can be readily reconfigured on demand to produce even more elaborate optical-field structures. To illustrate this capability, we generate a wavepacket involving a temporal train of three pulses, each assigned to a different spatial mode with a distinct prescribed frequency chirp, resulting in a non-separable wavepacket (Fig. 3). In this case, the spatial profiles allotted to the three pulses were intentionally chosen to match the LP $_{01}$, LP $_{11x}$ and LP $_{11y}$ fibre modes, with zero, positive and negative chirp, respectively, where LP $_{11x,y}\approx (LG_{+1}\mp LG_{-1})/\sqrt{2}$ and LG $_{\pm 1}$ are the OAM modes. In Fig. 3a, we display the measured iso-intensity profile of the generated ST wavepacket sequence, featuring the intensity patterns of the pre-engineered LP modes. A spectro-temporal map depicting the intensity and phase morphology of the field is shown in Fig. 3b. Enlarged intensity/phase profiles of the selected regions of this spectro-temporal map are exhibited in Fig. 3c, where we can clearly

observe the profiles of the LP modes at different temporal coordinates. The imposed linear frequency chirp for each pulse is clearly observed in the colour-coded modal decomposition map (Fig. 3d), where LP_{11x,v} represent positive/negative slopes and LP₀₁ has a zero chirp. In this spectrograph, the pink and cyan colours correspond to the LP_{11x} and LP_{11x} modes, respectively, generated as a linear combination of Laguerre modes $\ell = +1$ (red) and $\ell = -1$ (blue). The green colour ($\ell = 0$) corresponds to the LP₀₁ mode. We further exploit the full three-dimensional capabilities of our system by performing additional experiments using higher-order Hermite-Gauss orthogonal modes (Supplementary Section VIII). In view of the fact that the spatial modes generated here are exactly compatible with fibre systems, one may use this platform to mitigate mode group delay effects in multimode fibres, thus establishing new design paradigms for ultrafast fibre amplifiers. Furthermore, by optimizing the MPLC holograms⁴³ in our approach, we could potentially harness a larger bandwidth to produce an arbitrary sequence of ~11 fs spatiotemporal wavepackets centred around 1 µm. These same concepts can be readily extended to other wavelengths, for example, 0.5 µm and 1.5 µm, which are critical for technologies.

To further demonstrate the versatility of our system, we now synthesize three spatial vortex fields, namely, $\ell = -1$, 0, +1, precisely positioned at specific times. In this case, we perform a series of experiments where we control the relative delay between the modal components of the ST wavepacket. Figure 4a shows the obtained

NATURE PHOTONICS LETTERS

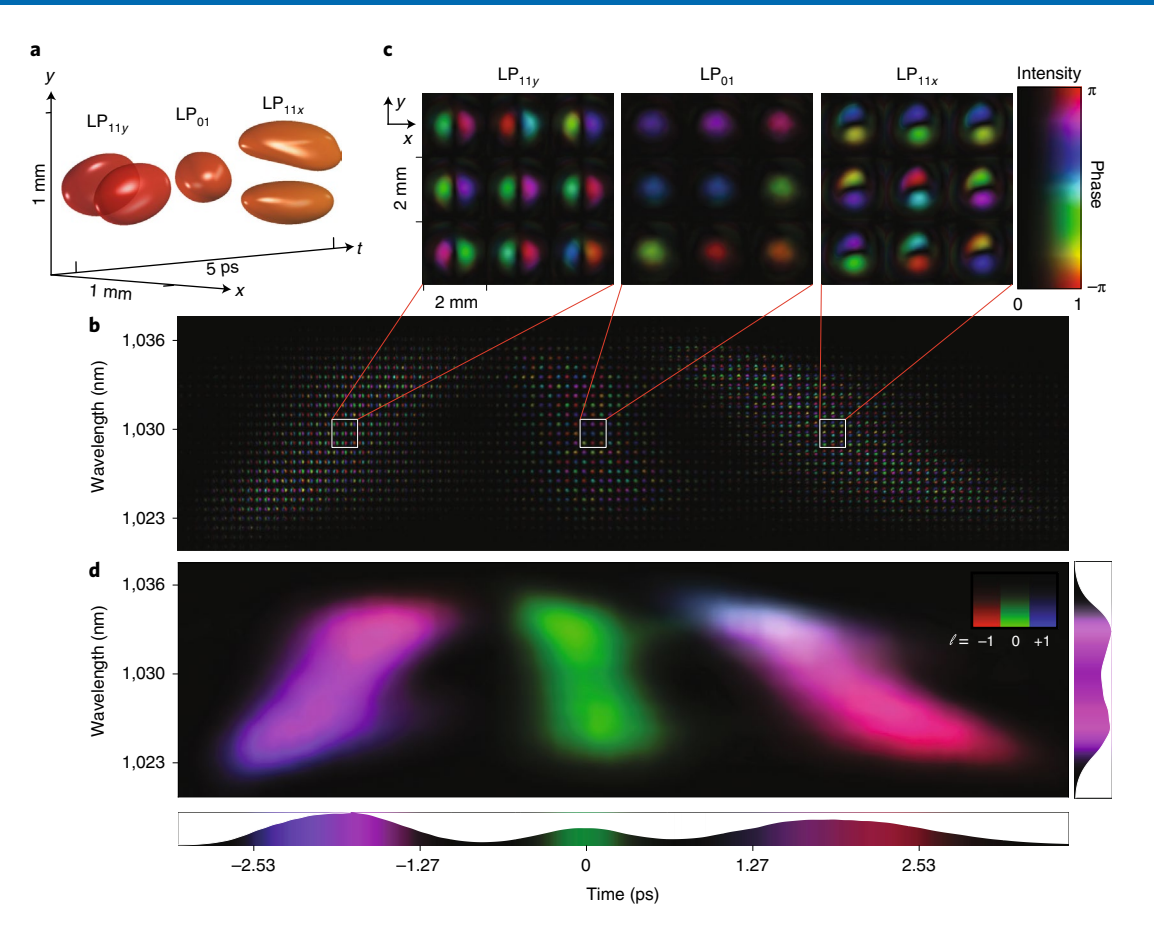


Fig. 3 | An optical wavepacket with an intricate ST texture. a, Measured iso-intensity profile of the synthesized wavepacket (at $I_{contour} = 0.5I_{max}$), exhibiting a dynamic spatial modal distribution. The generated field consists of a temporal train of three pulses, with each pulse exhibiting a specific frequency chirp and spatial beam profile. The LP_{11x} , LP_{01} and LP_{11x} spatial-mode structures are generated using the MPLC module (Fig. 1b). **b**, Spectro-temporal map with each 'pixel' corresponding to the spatial distribution of the amplitude and phase, measured at a specific time and wavelength. **c**, Expanded view of the field at selected points displaying the evolution of the intensity and phase distributions along the wavepacket. The amplitude is represented by brightness, whereas the phase is represented by colour, as indicated in the two-dimensional colour bar. **d**, Colour-coded modal decomposition map associated with a Laguerre–Gaussian basis, as shown in Fig. 2d. Here the linear frequency chirp for each pulse is clearly observed. The LP_{11xy} values exhibit positive/negative chirp slopes (purple colour). On the other hand, the LP_{01} component has no frequency chirp (green colour).

colour-coded modal decomposition maps for five consecutive measurements. For these realizations, the OAM modes ℓ_{-1} (red) and ℓ_{+1} (blue) remain stationary in time as we sweep the relative delay of the ℓ_0 (green) spatial mode. Note that in the ST wavepacket (Fig. 4a, top row), the ℓ_0 and ℓ_{-1} modes overlap temporally, thus producing the displayed yellow pattern. In Fig. 4a (second row), as the tailing edge of the ℓ_0 mode overtakes the ℓ_{+1} mode, the green, red and blue regions can be clearly observed in wavelength and time. In Fig. 4a (bottom row), the cyan pattern corresponds to the overlap of the ℓ_0 and ℓ_{+1} OAM modes.

In a series of experiments, we now judiciously assign specific spatial profiles and time delays to different slices of the pulse spectrum; we effectively demonstrate simultaneous control of the ST dimensions. For this purpose, we first synthesize an ST wavepacket engaging two distinct temporal pulses with different modal compositions. The spatial profile of the first pulse varies from an OAM state ℓ_0 to ℓ_{-1} on the short-/long-wavelength part of the spectrum. On the other hand, the second pulse exhibits ℓ_{-1} and ℓ_0 characteristics at long and short wavelengths, respectively. The measured modal decomposition (Fig. 4b, top row) reveals the successful generation of such an intricate electromagnetic structure. This is depicted via the assigned colour patterns (green/red and blue/green) on the modal decomposition map (Fig. 4, top row). We then sequentially displace—in both frequency and time—the OAM ℓ_{+1} and ℓ_{-1}

components, in such a way that the $\ell_{\pm 1}$ modes move towards each other, whereas the ℓ_0 mode remains stationary. During this evolution, the ℓ_{+1} and ℓ_{-1} states converge in wavelength and time, crossing over, as displayed by the purple pattern (Fig. 4b, middle row). After this crossover, the wavelength/time positions of the $\ell_{\pm 1}$ modes are inverted in the ST wavepacket. Supplementary Fig. 16 presents the measured iso-intensity profile of the generated ST wavepackets.

In summary, we have demonstrated ultrafast ST wavepackets with predefined multimodal, temporal and spectral composition on demand. Our system enables broad control of light's spatiotemporal DOFs, a valuable attribute that can be readily deployed over a wide range of applications. In this respect, this platform can be tailored, for example, to induce extreme nonlinear phenomena by means of OAM ST wavepackets and be instrumental in developing high-intensity ultrafast multimode fibre amplifiers. The methodology demonstrated here could have important implications in a number of scientific frontiers in chemistry and physics where ST control plays a key role.

Online content

Any methods, additional references, Nature Research reporting summaries, source data, extended data, supplementary information, acknowledgements, peer review information; details of author contributions and competing interests; and statements of

LETTERS NATURE PHOTONICS

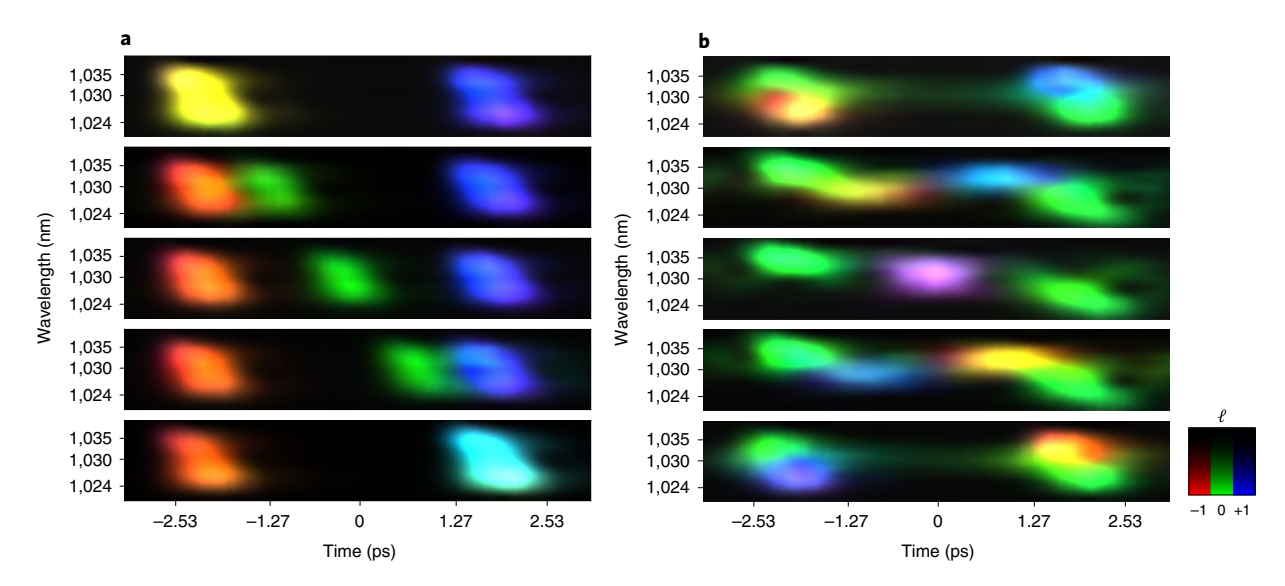


Fig. 4 | On-demand generation of spatiotemporal wavepackets. a, A sequence of spectro-temporal maps, demonstrating precise control of the temporal location of the spatial modes with $\ell=-1$, 0, +1. In this sequence, each OAM value is associated with RGB colours: $\ell=-1$ (red); $\ell=0$ (green); $\ell=+1$ (blue). In each row, the wavepacket consists of three pulses, which exhibit the same frequency chirp but different spatial profiles. The OAM components with ℓ_{-1} (red) and ℓ_{+1} (blue) remain stationary, whereas the ℓ_0 mode (green) is sequentially shifted in time. The experimentally observed temporal/frequency pulse overlap of the ℓ_{-1}/ℓ_0 and ℓ_0/ℓ_{+1} OAM structure is shown by the yellow and cyan regions, respectively. **b**, Spectro-temporal diagrams demonstrating control of the temporal, spectral and spatial properties of the field. Initially, two pulses are generated at different times (top row). The first pulse is composed of ℓ_0 and ℓ_1 vortex modes (red/green) assigned to different sections of its spectrum, whereas the second pulse involves ℓ_{+1} and ℓ_0 modes (green/blue) for the corresponding frequencies. The ℓ_1 and ℓ_1 elements are sequentially adjusted in time and frequency, whereas ℓ_0 remains stationary. The subsequent rows display the time and frequency translation of the ℓ_1 and ℓ_1 components diagonally across the spectro-temporal window.

data and code availability are available at https://doi.org/10.1038/s41566-022-01055-2.

Received: 9 January 2022; Accepted: 7 July 2022; Published online: 29 August 2022

References

- 1. Kerse, C. et al. Ablation-cooled material removal with ultrafast burst pulses. *Nature* **537**, 84–88 (2016).
- Malik, M. et al. Multi-photon entanglement in high dimensions. Nat. Photon. 10, 248–252 (2016).
- Mair, A., Vaziri, A., Weihs, G. & Zeilinger, A. Entanglement of the orbital angular momentum states of photons. *Nature* 412, 313–316 (2001).
- Wang, J. et al. Terabit free-space data transmission employing orbital angular momentum multiplexing. Nat. Photon. 6, 488–496 (2012).
- Li, L. et al. High-capacity free-space optical communications between a ground transmitter and a ground receiver via a UAV using multiplexing of multiple orbital-angular-momentum beams. Sci. Rep. 7, 17427 (2017).
- Teğin, U., Yıldırım, M., Oğuz, İ., Moser, C. & Psaltis, D. Scalable optical learning operator. Nat. Comput. Sci. 1, 542–549 (2021).
- Teğin, U., Yıldırım, M., Oğuz, İ, Moser, C. & Psaltis, D. Machine learning with multimode fibers. In 2021 Conference on Lasers and Electro-Optics (CLEO) 1–2 (IEEE, 2021).
- Wetzstein, G. et al. Inference in artificial intelligence with deep optics and photonics. Nature 588, 39–47 (2020).
- Lin, D. et al. Reconfigurable structured light generation in a multicore fibre amplifier. Nat. Commun. 11, 3986 (2020).
- Wright, L., Cristodoulides, D. N. & Wise, F. W. Spatiotemporal mode-locking in multimode fiber lasers. *Science* 358, 94–97 (2017).
- 11. Malomed, B. A., Mihalache, D., Wise, F. & Torner, L. Spatiotemporal optical solitons. *J. Opt. B: Quantum Semiclass. Opt.* 7, R53–R72 (2005).
- Dolev, I., Kaminer, I., Shapira, A., Segev, M. & Arie, A. Experimental observation of self-accelerating beams in quadratic nonlinear media. *Phys. Rev. Lett.* 108, 113903 (2012).
- Fleischer, A., Kfir, O., Diskin, T., Sidorenko, P. & Cohen, O. Spin angular momentum and tunable polarization in high-harmonic generation. *Nat. Photon.* 8, 543–549 (2014).
- 14. Gariepy, G. et al. Creating high-harmonic beams with controlled orbital angular momentum. *Phys. Rev. Lett.* **113**, 153901 (2014).
- Rego, L. et al. Generation of extreme-ultraviolet beams with time-varying orbital angular momentum. Science 364, eaaw9486 (2019).

- Dorney, K. M. et al. Controlling the polarization and vortex charge of attosecond high-harmonic beams via simultaneous spin-orbit momentum conservation. Nat. Photon. 13, 123–130 (2019).
- Rego, L. et al.Generation of extreme-ultraviolet beams with time-varying orbital angular momentum. Science 364, eaaw9486 (2019).
- Piccoli, R. et al. Intense few-cycle visible pulses directly generated via nonlinear fibre mode mixing. Nat. Photon. 15, 884–889 (2021).
- 19. Liu, X., Du, D. & Mourou, G. Laser ablation and micromachining with ultrashort laser pulses. *IEEE J. Quantum Electron.* **33**, 1706–1716 (1997) .
- Kraus, M. et al. Microdrilling in steel using ultrashort pulsed laser beams with radial and azimuthal polarization. Opt. Express 18, 22305–22313 (2010)
- Heritage, J. P., Weiner, A. M. & Thurston, R. N. Picosecond pulse shaping by spectral phase and amplitude manipulation. Opt. Lett. 10, 609–611 (1985).
- Thurston, R., Heritage, J., Weiner, A. & Tomlinson, W. Analysis of picosecond pulse synthesis by spectral masking in a grating pulse compressor. *IEEE J. Quantum Electron.* 22, 682–696 (1986).
- Durnin, J., Miceli, J. J. Jr. & Eberly, J. H. Diffraction-free beams. *Phys. Rev. Lett.* 58, 1499 (1987).
- Bandres, M. A., Gutierrez-Vega, J. C. & Chavez-Cerda, S. Parabolic nondiffracting optical wave fields. Opt. Lett. 29, 44–46 (2004).
- Kaminer, I., Bekenstein, R., Nemirovsky, J. & Segev, M. Nondiffracting accelerating wave packets of Maxwell's equations. *Phys. Rev. Lett.* 108, 163901 (2012)
- Siviloglou, G. A., Broky, J., Dogariu, A. & Cristodoulides, D. N. Observation of accelerating Airy beams. *Phys. Rev. Lett.* 99, 213901 (2007).
- Yao, A. M. & Padgett, M. J. Orbital angular momentum: origins, behavior and applications. Adv. Opt. Photon. 3, 161–204 (2011).
- Brittingham, J. N. Focus waves modes in homogeneous Maxwell's equations: transverse electric mode. J. Appl. Phys. 54, 1179–1189 (1983).
- Chong, A., Renninger, W. H., Christodoulides, D. N. & Wise, F. W. Airy–Bessel wave packets as versatile linear light bullets. *Nat. Photon.* 4, 103–106 (2010).
- Kondakci, H. E. & Abouraddy, A. F. Diffraction-free space-time light sheets. Nat. Photon. 11, 733–740 (2017).
- Kondakci, H. E. & Abouraddy, A. F. Optical space-time wavepackets having arbitrary group velocities in free space. *Nat. Commun.* 10, 929 (2019).
- Yessenov, M. et al. Space-time wave packets localized in all dimensions. Preprint at https://arxiv.org/abs/2111.03095 (2021).
- Chong, A., Wan, C., Chen, J. & Zhan, Q. Generation of spatiotemporal optical vortices with controllable transverse orbital angular momentum. *Nat. Photon.* 14, 350–354 (2020).

NATURE PHOTONICS LETTERS

- Cao, Q. et al. Sculpturing spatiotemporal wavepackets with chirped pulses. Photon. Res. 9, 2261–2264 (2021).
- 35. Wan, C., Chen, J., Chong, A. & Zhan, Q. Photonic orbital angular momentum with controllable orientation. *Natl Sci. Rev.* nwab149 (2021).
- Chen, J., Wan, C., Chong, A. & Zhan, Q. Experimental demonstration of cylindrical vector spatiotemporal optical vortex. *Nanophotonics* 10, 4489–4495 (2021).
- Wan, C., Chen, J., Chong, A. & Zhan, Q. Generation of ultrafast spatiotemporal wave packet embedded with time-varying orbital angular momentum. Sci. Bull. 65, 1334–1336 (2020).
- 38. Wan, C., Cao, Q., Chen, J., Chong, A. & Zhan, Q. Photonics toroidal vortex. Preprint at https://arxiv.org/abs/2109.02833 (2021).
- Zdagkas, A. et al. Observation of toroidal pulses of light. Preprint at https://arxiv.org/abs/2102.03636 (2021).
- 40. Mounaix, M. et al. Time reversed optical waves by arbitrary vector spatiotemporal field generation. *Nat. Commun.* 11, 5813 (2020).
- Baxter, G. et al. Highly programmable wavelength selective switch based on liquid crystal on silicon switching elements. In 2006 Optical Fiber Communication Conference and the National Fiber Optic Engineers Conference 1–3 (IEEE, 2006).

- 42. Morizur, J. F. et al. Programable unitary spatial mode manipulation. *J. Opt. Soc. Am. A* 27, 2524–2531 (2010).
- Fontaine, N. K. et al. Laguerre-Gaussian mode sorter. Nat. Commun. 10, 1865 (2019).
- 44. Gabolde, P. & Trebino, R. Self-referenced measurement of the complete electric field of ultrashort pulses. *Opt. Express* 12, 4423–4429 (2004).
- Gabolde, P. & Trebino, R. Single-frame measurement of the complete spatiotemporal intensity and phase of ultrashort laser pulses using a wavelengthmultiplexed digital holography. J. Opt. Soc. Am. B 25, A25–A33 (2008).
- Kimel, I. & Elias, L. R. Relations between Hermite and Laguerre Gaussian modes. IEEE J. Quantum Electron. 29, 2562–2567 (1993).

Publisher's note Springer Nature remains neutral with regard to jurisdictional claims in published maps and institutional affiliations.

Springer Nature or its licensor holds exclusive rights to this article under a publishing agreement with the author(s) or other rightsholder(s); author self-archiving of the accepted manuscript version of this article is solely governed by the terms of such publishing agreement and applicable law.

© The Author(s), under exclusive licence to Springer Nature Limited 2022

LETTERS NATURE PHOTONICS

Methods

We employ a pulse laser source centred at ~1,030 nm, 180 fs (~6.4 nm FWHM; sech²-shaped pulse) and repetition rate of 40 MHz (Origami NKT Photonics). The beam is controllably divided into reference and signal pulses using a half-wave plate (AHWP05M-980, Thorlabs) and a polarization beamsplitter (PBS123, Thorlabs). The signal pulse train is temporally modulated by a two-dimensional Fourier-transform pulse shaper in a folded configuration. We use a ruled reflective diffraction grating (1,200 grooves mm⁻¹ and blaze wavelength of 1 µm; Thorlabs). A C-coated cylindrical lens with 30 cm focal length (LJ1558RM-B, Thorlabs). Additionally, we employ a $1,920 \times 1,080$ pixels reflective SLM with a pixel size of 8 µm (PLUTO-2.1-NIR HOLOEYE). The modulated pulse coming out of the two-dimensional Fourier-transform pulse shaper is directed to the next stage by a 50/50 beamsplitter (BS014, Thorlabs). The size of the field is adjusted with a two-lens system composed of two C-coated planoconvex lenses, namely, $f_1 = 3.5$ cm (LA1027-C, Thorlabs) and $f_2 = 30.0$ cm (LA1484-C, Thorlabs). At the last stage, we spatially engineer the field profile with an MPLC system using a 1,920 × 1,080 pixels reflective SLM with a pixel size of 8 µm (PLUTO-2.1-NIR, HOLOEYE) and a squared mirror (PFSQ05-03-P01, Thorlabs).

To analyse the spatiotemporal structure of the synthesized fields, we use the reference pulse with a controllable time delay. To adjust the reference pulse's intensity, a second set of half-wave plate and polarization beamsplitter is used. We resolve the frequency components of the signal pulse by employing a spectral filter centred at 1,047.1 nm with 4 nm FWHM bandwidth (LL01-1047-12.5, Semrock) mounted on a rotation stage (ELL14, Thorlabs). The reference and signal arms are recombined using a 50/50 beamsplitter (BS005, Thorlabs). Finally, we record the reference and signal interference pattern on a CCD camera (2,048 \times 1,088 pixels, 5.5 μ m pixel size; BEAMAGE-3.0, Gentec). To capture the dynamics of the field, a linear translation stage is driven by an actuator (Z825B, Thorlabs). The time dimension is scanned by introducing time delay τ on the reference arm at time steps of \sim 66.66 ps (steps of 20 μ m optical path length), whereas the frequency components are interrogated by rotating the spectral filter at angle steps of 0.5° (Supplementary Sections II–V).

Data availability

All data that support the findings of this study are available within the paper and the Supplementary Information and are available from the corresponding author upon request.

Code availability

All the relevant computing codes used in this study are available from the corresponding author upon reasonable request.

Acknowledgements

This effort was sponsored, in part, by the Department of the Navy, Office of Naval Research, (N00014-20-1-2789); the National Science Foundation (EECS-1711230); the Simons Foundation (733682); the US-Israel Binational Science Foundation (BSF; 2016381); the Army Research Office of Scientific Research (W911NF1710553 and W911NF1910426); and NASA (80NSSC21K0624).

Author contributions

All authors contributed to all aspects of this work. D.C.D. performed the experiments in consultation with all the team members.

Competing interests

The authors declare no competing interests.

Additional information

Supplementary information The online version contains supplementary material available at https://doi.org/10.1038/s41566-022-01055-2.

Correspondence and requests for materials should be addressed to Rodrigo Amezcua-Correa or Miguel A. Bandres.

Peer review information *Nature Photonics* thanks Jose Azana, Pierre Bejot and the other, anonymous, reviewer(s) for their contribution to the peer review of this work.

Reprints and permissions information is available at www.nature.com/reprints.